4. Earth and sea sciences infrastructure

The Earth-Sea Science infrastructure is designed to be site independent to ensure the experienced gained in building and operating the node can be shared by future cabled observatory programmes around Europe. As a result this report deals with the seafloor infrastructure and not the instrumentation.

The list of functions of an ESONET/EMSO subsea observatory will be either shared with KM3Net telescope *(Shared)* or provided by the KM3Net telescope *(telescope)* or specific to the Earth-Sea science segments *(Specific)*:

The functions and components of a subsea observatory are:
1) Management of the infrastructure *(Specific)*
2) Dissemination and user interfaces *(Specific)*
3) Data bases *(Specific)*
4) Technical supervision infrastructure *(Specific)*
5) Onshore network *(Specific)*
6) Land Base termination of sea infrastructure *(telescope)*
7) Land sea communication segment *(Shared)*
8) Node from branching unit to Main junction box *(Shared)*
9) Branch extension of the network - uplink *(Specific)*
10) Secondary junction box *(Specific)*
11) Link to instruments - downlink *(Specific)*
12) Individual instrument *(Specific)*

The following sections describe components 9 to 11

4.1 General description

The Earth-Sea Science node will be connected to the KM3NeT main electro-optical cable via a primary junction box to which up to three secondary junction boxes, distributed around the neutrino telescope, will provide the required infrastructure.
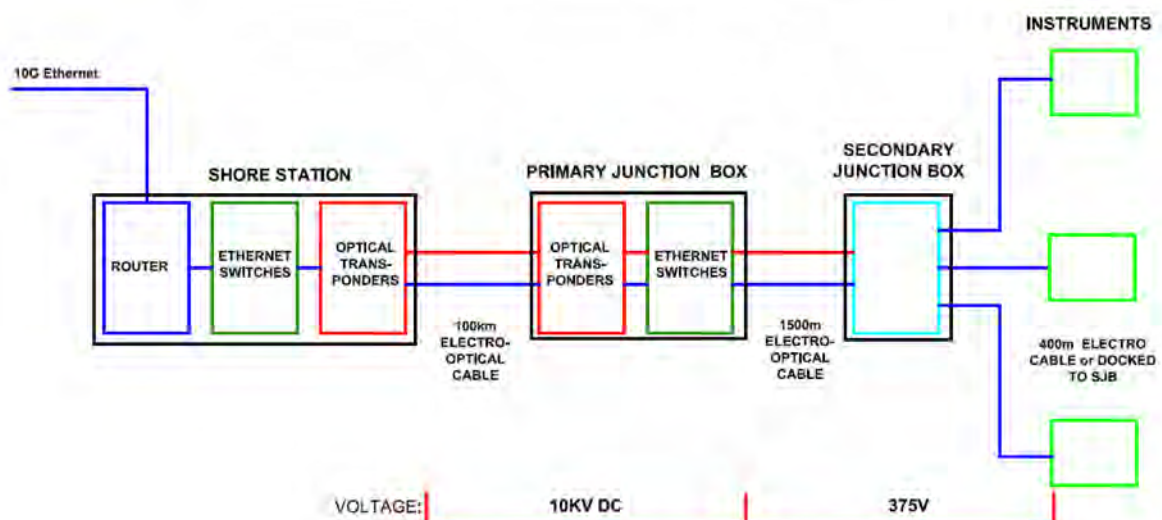

Figure 4-1: KM3NeT Earth-Sea Science node Network Architecture.

This infrastructure may consist of combinations of the following:

· Lines of autonomous sensors such as seismographs

· Moorings containing suites of instruments to monitor surface water, water column, sea bed and sub sea-floor

· Fixed structures with removable modules containing instruments such as cameras and flash lights, acoustic sensors and suites of oceanographic sensors such as the proposed ESONET standard instrumentation module

The electro optical cable and primary junction box will have identical specifications to those of the neutrino telescope and will be part of the common infrastructure. The secondary junction boxes however will have different requirements and will therefore be specific to the Earth-Sea science infrastructure.

The optimal layout of the Earth-Sea Science cable would be circular around the foot print of the telescope array however that will depend on the topology, telescope expansion plans and costs.

4.2 Junction box

The KM3NeT Earth-Sea science junction box will be based on the commercial junction box designed by OceanWorks International for the Neptune Canada deep-sea observatory. Some parts of the design may, however, need changing in order to meet the KM3NeT requirements.

The network architecture for the Earth-Sea science node is shown in Figure 4-1.
Note that in this architecture the node is the equivalent of the KM3NeT primary junction box and the primary junction box is the equivalent of the Earth-Sea science secondary junction box. The instruments are connected to the OceanWorks International junction box shown in Figure 4-2.

Figure 4-2: OceanWorks International Junction box.

The junction box supports a maximum of ten downlink interfaces and one uplink interface. It receives an input of 300-400 volts DC at up to 22 5 amps on the uplink interface from which all external and internal loads are powered.

The 400V power bus is referenced to seawater ground at the node such that two power leads are nominally +200V and -200V with respect to sea water. In case of a seawater ground fault, the junction box is designed to continue operating on either of the lines. The uplink power conductors have an isolation potential of at least 600V from seawater or pressure case. Figure 4-3 shows the Neptune Canada infrastructure.
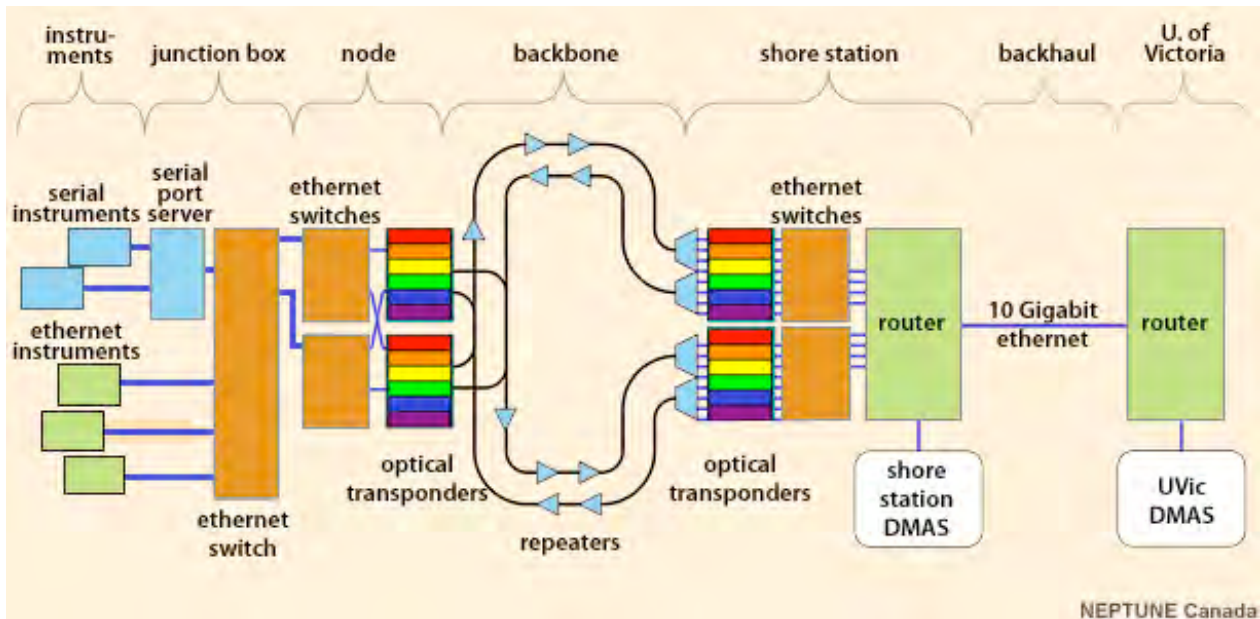
Figure 4-3: Neptune Canada Network architecture from data centre to instrumentation.

Cable Interface

The communications interface for the uplink interface is provided via one of the following:

· 100Base-T Ethernet;

· 1000Base-LX Ethernet on two single mode fibres;

· Dual 1000Base-LX Ethernet Links using four single mode fibres.

Each downlink provides a DC power supply circuit and a communications link which may consist of a combination of the following:

· Up to 600 watts at 48 volts;

· Up to 75 watts at 12V, 15V, 24V or 48V;

· Up to 150 watts at 24V or 48V;

· Other power levels at 12V, 15V, 24V or 48V are determined by the thermal limitations within the junction box;

· 10/100Base-T Ethernet;

· EIA-232, EIA-422 or EIA-485 serial data at up to 115.2 Kb/s;

· 1000Base-LX Ethernet.

The Ethernet uplinks comply with IEEE 802.3-2005 protocol. Optical uplinks consist of one or two bi-directional 1000Base-LX, each using two single mode fibres for a total of two or four fibres and support IEEE 802.3ad Link Aggregation Control Protocol (LAPC). Each Ethernet downlink interface supports one 100Base-T communications link compatible with any of the following output voltage levels: 12V, 15V, 24V, 48V, 300 to 400V. Each signal line is transformer coupled to maintain isolation in the event of a connector leak. They are IEEE 802.3-2005 compliant. Each junction box has a maximum of four serial communications downlink interfaces to connect the instruments. They support one of EIA-232, EIA-422, or EIA-485 communication link at operating up to 115.2 kb/s. The interface is software configurable. Each serial downlink interface is compatible with any of the following output power voltage levels 12V, 15V, 24V, 48V, 300-400V. Each signal line is optically isolated to maintain isolation in the event of a connector failure.

Downlink power conductors have an isolation potential of at least 100V from seawater or pressure housing. Conductors enter the pressure vessel through a Seacon MINK-10 (2#14, 8#20)-FCRL-TI penetrator.

Each junction box allows for the addition of two optical downlink interfaces supporting one 1000Base-LX Ethernet communications link and compatible with any of the following output power levels: 12V, 15V, 24V, 48V, 300-400V.

Conductors and fibres for an optical downlink enter the pressure vessel through an ODI Hybrid Bulkhead Penetrator having a 1.312 inch diameter bore and a 3 inch diameter flange. The Ethernet downlinks comply with IEEE 802.3-2005.

Communications Interface

The communications switch is equipped with a fully managed Ethernet switch or multiple connected switches to satisfy the number of interfaces. The switch is software configurable and can be accessed via remote control either via telnet or http. It can also be up-graded remotely.
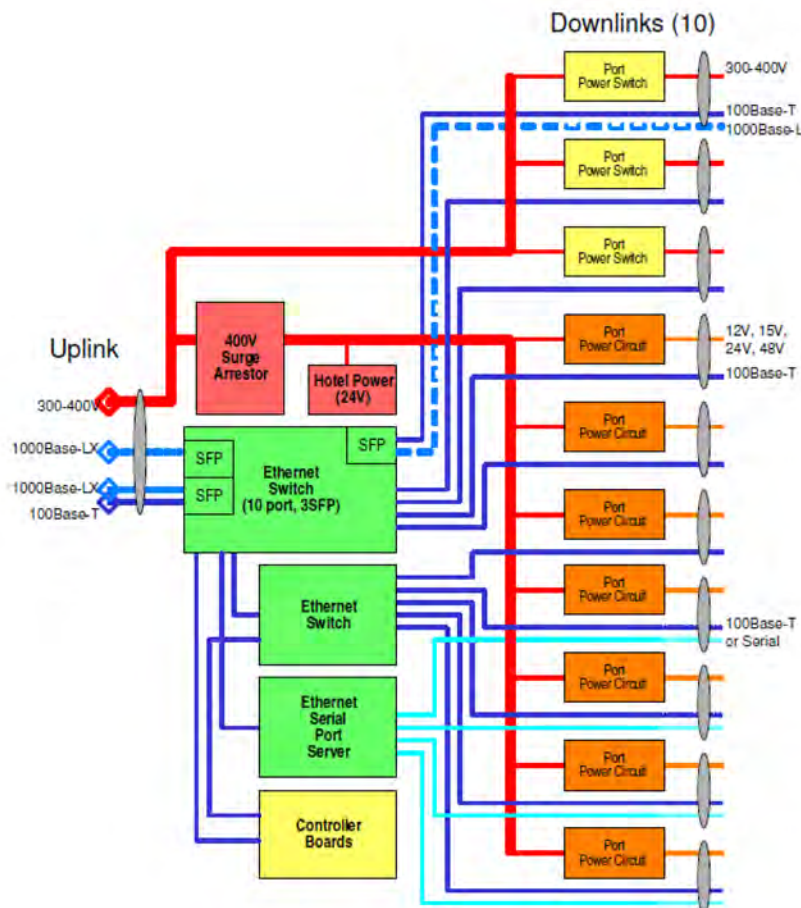

Figure 4-4: OceanWorks junction box block diagram.

The junction box supports IPv4 and IPv6 internet protocols. It tolerates a bit error rate for underwater interface to shore interface link of 1×10^{-12} or the equivalent packet loss rate of $1\ 2 \times 10^{-8}$. The Junction box switches support IEEE 802.1Q virtual local area network tagging for data routing and prioritisation, IP multicast and IEEE 802.3ad link aggregation control protocol on the 1000Base-LX uplinks only. The junction box controller uses TCP/IP or UDP only (IP broadcast is only ever used for address resolution).

The junction box is equipped with one or more fully managed Ethernet Serial Server(s) (ESS) satisfying the number of interfaces. Where instrumentation is limited to serial communications only, the data is encapsulated in IP for transmission to the shore station using the ESS. The ESS software can be reconfigured or upgraded remotely via telnet. Figure 4-4 depicts a block diagram of the Ocean-works junction box.

Electrical interface

The junction box supports a maximum of three interfaces. Each interface is capable of 15 A output at 300-400V.
At least one interface per junction box shall support a 600 watt output at 48V.

The available electrical interface configurations are as follows:
• 15 A at 300-400 V;
• 600 W at 48 V;
• 150 W at 48 V;
• 150 W at 24 V;
• 75 W at 12 V;
• 75 W at 15 V;
• 75 W at 24 V;
• 75 W at 48 V.

The voltage regulation from no load to full load steady state is better than 1%. Interfaces supporting other power levels can be supported provided the thermal design of the junction box can accommodate them.
The voltage level received on the uplink interface is delivered to any 300-400V output and is not required to be stabilized or adjusted. The voltage converter efficiency is 80% or better at full load.

The junction box is designed such that a dead short applied to any downlink interface will not cause permanent damage to any other interface. Both power and return paths are isolated from seawater and neither the metal chassis nor the pressure housing is used as the current return path. There is no low resistance connection between either side of the power supply or any communications line and the ground within the junction box.
The junction box has active and passive surge arresting capability to prevent overvoltage up to 800 V on any 400 V uplink or downlink from damaging the junction box components. Peak voltage, peak current and maximum energy dissipation are to be confirmed.
Mechanical and Environmental Interfaces
The junction box enclosure provides a 1 Bar air-purged environment for the internal components. The housing is designed for a fifteen year operational life cycle of continuous sea water submersion with no degradation to system performance. Provision is made to recover the junction box every five years for refurbishment and redeployment. The operational depth of the junction box is 3000 m and may need to be upgraded.
The junction box is designed to operate in ambient water temperatures down to 3˚C and be able to tolerate temperatures of between -20˚C and 70˚C during transport and installation.

Operational and Control Procedures

The junction box is operated continuously and reports its status on a regular basis as well as on request. The junction box will start up automatically once power is provided either from a primary or another secondary junction box. It returns to a safe state when power is withdrawn.

Each instrument is monitored for power consumption and fault diagnostics. The following are measured and reported by the junction box at a rate of at least 1 Hz:

• Voltage levels on 12 V, 15 V, 24 V and 48 V outputs with a 100 mV resolution and a ± 0 5 V accuracy;

• Current levels on all outputs are measured with a resolution of 20 mA and ±100 mA accuracy;

• Ground faults with resistances between 5 kΩ and 5 MΩ shall be detected on the 12 V, 15 V, 24 V and 48 V outputs with an accuracy of ±20 % ;

• Alarm thresholds for each interface shall be configurable via software.

Each interface can be remotely disabled to prevent damage to the junction or other instrumentation and re-enabled once problems have been solved. In such instances power and communication lines are isolated such that they provide no current path from any external connector pin to any internal component or chassis. The temperature within the junction box housing shall be monitored with a resolution of ±1˚C. The junction box input power supply is measured and monitored with ±1 V accuracy.

Data is transmitted via a continuous UDP stream at a rate of at least 1 Hz. The junction box is equipped with a controller to communicate with the control centre, monitor interfaces and internal sensors, and control the interfaces. The controller has an IP address, is software configurable and can be controlled and upgraded remotely. The junction box responds to commands sent asynchronously from the shore station such as requests for status information and data transmission. Command execution is always acknowledged. The junction box internal clock can be set by command to within 2 seconds accuracy. There is no requirement for the junction box to pass timing signals to the instruments. Instruments are required to acquire timing signals using network time protocol or precision time protocol. The junction box provides a means of locating and isolating faults in internal components, including but not limited to power converters, optical transmitters and receivers, switches, ESS, and other communications equipment, without underwater intervention. Performance, fault, configuration and security information is transmitted to the shore station.

Estimates of the overall reliability based on components, sub-assembly, or sub-system reliability data and using appropriate calculations or modelling are included. They are calculated based on Telcordia, MIL-HDBK-217F, or other recognised standards. FIT (Failure in Time) & MTBF (Mean Time Between Failure) figures are provided together with their source. The probability of complete failure within the first year of operation does not exceed 10% where complete failure means a failure of all junction box ports. Assuming there are no duplicated or redundant components within the instrument, this probability of failure is equivalent to a total FIT for core components of 12,000 or less where core components are those whose failure would cause all ports to become unusable.

For a system with no redundant components, FIT and probability of failure over a given time period are mathematically linked as follows:

$MTBF$ ($hours$) = 10^9 / FIT;

$MTBF$ ($years$) = $MTBF$ ($hours$) / 8760;

The failure rate: R_{fail} = 1 /$MTBF$;

The failure probability in time t: is given by $P_{fail}(t) = 1 - e^{-R_{fail}t}$.

4.3 Connectivity

The earth-Sea science node consists of several electrical, mechanical and power components which need to meet deployment, safety and environmental constraints and will likely vary depending on the final site selection. This section identifies the components individually and suggests technologies that may be used to address the safety and environmental requirements. A block diagram representing these components is shown in Figure 4-5.

4.3.1 Main Uplink Cable

This cable must be compatible with KM3NeT neutrino telescope which currently is in the order of 400 V input delivering in the order of 125 kW power of which 10 kW is reserved for the Earth-Sea science node.
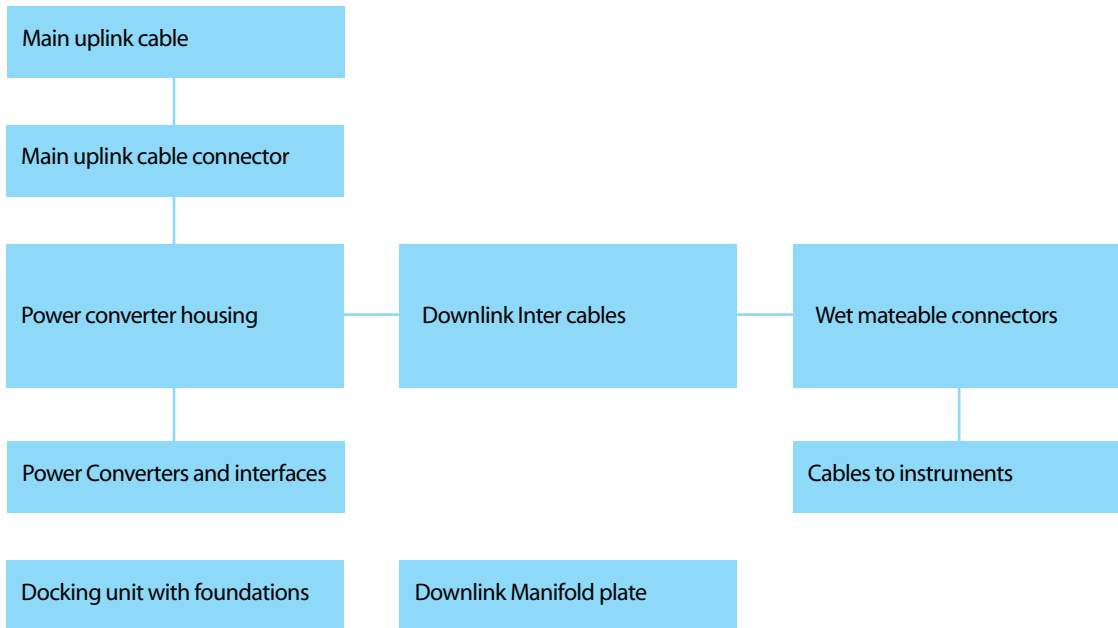
```
┌─────────────────────────────┐
│  Main uplink cable          │
└─────────────────────────────┘
              │
┌─────────────────────────────┐
│  Main uplink cable connector│
└─────────────────────────────┘
              │
┌──────────────────────┐   ┌──────────────────────┐   ┌──────────────────────┐
│ Power converter      │───│ Downlink Inter cables│───│ Wet mateable         │
│ housing              │   │                      │   │ connectors           │
└──────────────────────┘   └──────────────────────┘   └──────────────────────┘
              │                                                    │
┌──────────────────────┐                              ┌──────────────────────┐
│ Power Converters and │                              │ Cables to instruments│
│ interfaces           │                              │                      │
└──────────────────────┘                              └──────────────────────┘

┌──────────────────────┐   ┌──────────────────────┐
│ Docking unit with    │   │ Downlink Manifold    │
│ foundations          │   │ plate                │
└──────────────────────┘   └──────────────────────┘
```

Figure 4-5: Earth-Sea Science node component breakdown.

4.3.2 Uplink Cable connection

This may be a wet or dry mated connection depending on deployment method and available technology.

4.3.3 Power Converter and interfaces

These are similar to the Neptune Canada power-system requirements and if possible have the option to be reconfigurable as the instrumentation changes over the 20 year life cycle of the observatory.

4.3.4 Downlink Cables

Options may be to install the cables with dry mateable connectors or oil filled tubes on deck before deployment of the junction box.

4.3.5 Connector Manifold plate

This could be like an ROV tool plate with wet mateable connectors. Recommendation for parameters such as the distance between connectors and grabbing pressure will be set for the design and included in the operation guide. The connectors and associated hardware can be spaced at a given distance apart and a given height above the sea floor. It will require a grab bar for ROV operations with the grab.
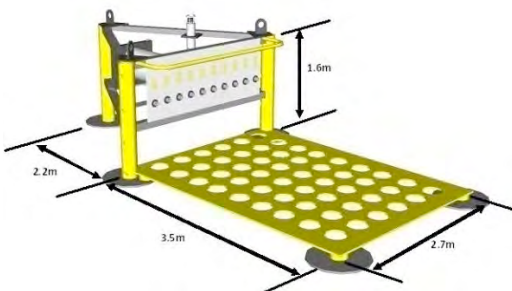
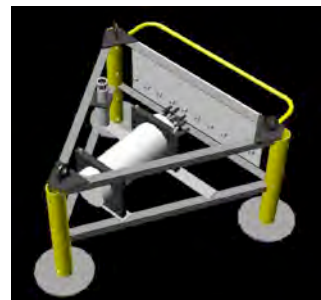*Figure 4-6: Docking unit with foundations and approximate dimensions.*

Figure 4-7: Sketch of junction box frame.

4.3.6 Docking Unit with foundations

The experience with subsea observatories used for Earth-Sea science as well as neutrino telescope first generation projects demonstrated the need to offer an easy interface for connection with an ROV. The connecting phase is critical for the reliability of the whole infrastructure.

A docking underwater structure supports the secondary Junction box and allows for easy access to any of the connectors with well defined coordinates, thus enabling the operation of the ROV according to well defined procedures. Figure 4-6 and Figure 4-7 give an impression of the dimensions of such a junction.

4.4 Deployment and Maintenance

Most components will be commercially available and therefore testing certificates will be provided on delivery demonstrating, where necessary, results of the relevant quality control tests. If a different use from the operational references of the sensor or component is foreseen, the instrument may be validate on an Earth-Sea Science test bed in a laboratory or using a sea-bed test node developed by the ESONET Network of Excellence.

4.5 Marine Operations

All Earth-Sea science data obtained from both the science node and instruments positioned within the array for calibration purposes will be made available to the science community, government agencies, outreach programmes and monitoring agencies. The raw data will be stored in real time at the shore station and disseminated according to the ESONET data management methods as shown in Figure 4-8, complying with GMES-GEOSS, INSPIRE and other policies on ocean environment. Existing data networks and data centres will be used to provide access for registered users. When the background knowledge is sufficient, standard data quality checks will be performed prior to distribution. Further processing may be done at the holding data centres.

4.6 Additional Features

Together with the ESONET group working on smart sensors, Ifremer proposed an adapted secondary junction box specification. It takes into account the advances of technology since the Neptune Canada design, additional operational constraints for the KM3NeT project and enhances the versatility.

A major input took its root in the KM3Net project thanks to the technological comparison of potential technologies for the downlink between secondary junction box and instrumentation (cf NIKHEF studies). Both fibre-optic communication and VDSL2 communication on twisted pairs are capable of the high data transmission rate.

A project called DeepSeaNet involving a low cost fibre optic solution without the need for power transmission will also be considered. It will allow the collection of data from areas several kilometres away from the KM3NeT site, such as zones threatened by geo-hazards. Validation of this technology is taking place in 2010 at the Antares site.

A low cost connection will also be implemented, allowing for the hosting of experiments without requiring the purchase of expensive connectors. This feature has been demonstrated during several projects (such as the FP5 Assem project [24]) and will be implemented at Antares and Neptune Canada.
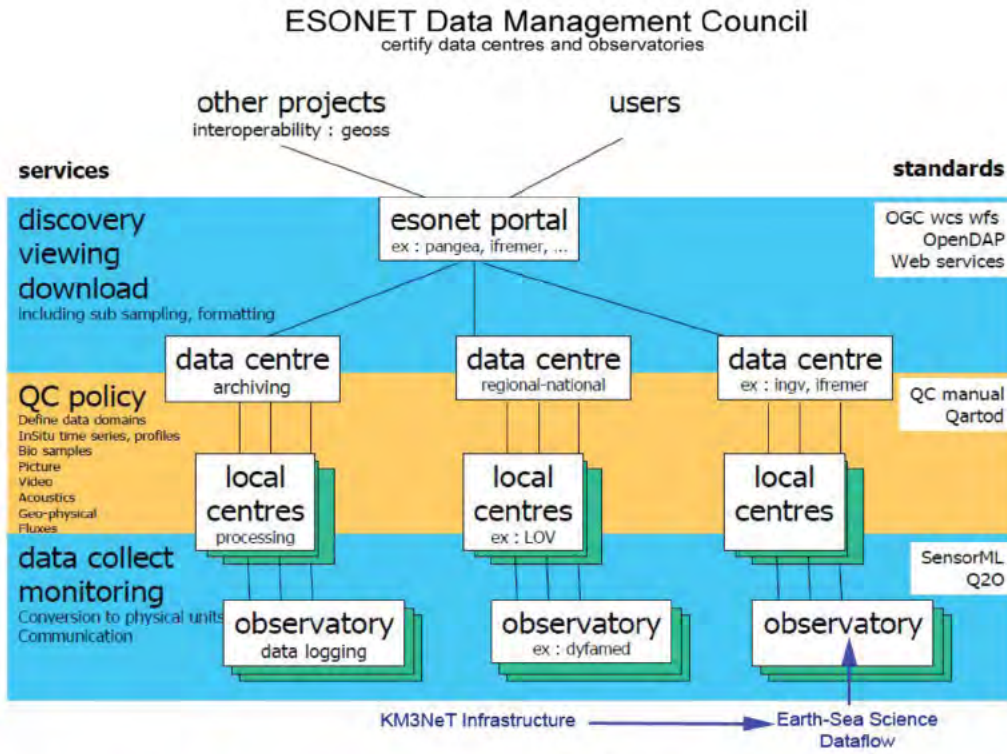
Figure 4-8: KM3NeT Earth-Sea Science dataflow with respect to ESONET data management plan.

5. Site Characterisation

The Mediterranean Sea offers optimal conditions, on a worldwide scale, to host an underwater neutrino telescope. Several suitable sites have been identified and their physical, geophysical and oceanographic properties investigated in detail. In the following, the most relevant results of these studies are presented. In assessing them, it has to be kept in mind that measurements have been performed with different devices and at different points in time.

The most relevant requirements for candidate sites to host the KM3NeT infrastructure are:
- Proximity to coast to ease deployment and reduce the expense of the power and signal cable connections to shore;
- Sufficient depth to fully shield the day light and reduce background from atmospheric muons, in particular from those that are falsely reconstructed as up-going;
- Good optical properties of the water, i.e. absorption and scattering lengths close to the ones of optically pure sea water for light in the wavelength range of about 350 nm to 550 nm;
- Low level of bioluminescence;
- Low rate of biofouling (bacterial film deposition and marine life accretion) on optical surfaces;
- Low rate of sedimentation;
- Low sea current velocities;
- Low risk of significant seismic events.

A geographic information system tool has been developed that allows parameters such as depth, distance from shore, costs, water properties to be given a weighting to help with site selection. An in depth description of the method and its flexibility is given [25].

5.1 Locations
The ANTARES, NEMO and NESTOR Collaborations have carried out dedicated research programmes to characterise the candidate sites, which are currently pursued within the context of the KM3NeT project. The locations of the three candidate regions, shown in Figure 2-2 are:

Toulon - Ligurian Sea (ANTARES):
- 42°48′ N 06°10′ E; depth: 2475 m; cable length to shore 40 km.

Capo Passero - West Ionian Sea (NEMO):
- 36°16′N 16°06′E; depth: 3500 m; cable length to shore 100 km.

Pylos - East Ionian Sea (NESTOR):
- 36°33′N 21°08′E; depth: 5200 m; cable length to shore 50 km;

- 36°33′N 21°29′E; depth: 4500 m; cable length to shore 30 km;

- 36°38′N 21°35′E; depth: 3750 m; cable length to shore 20 km;

- 36°50′N 21°32′E; depth: 3000 m; cable length to shore 15 km.

5.1.1 Bathymetry

The topology of the seafloor has been measured for all three candidate site regions, see for instance Figure 5-1 for the Pylos site and Figure 5-2 for the Toulon site. These measurements show that sufficiently large, approximately plane areas are available at each site.
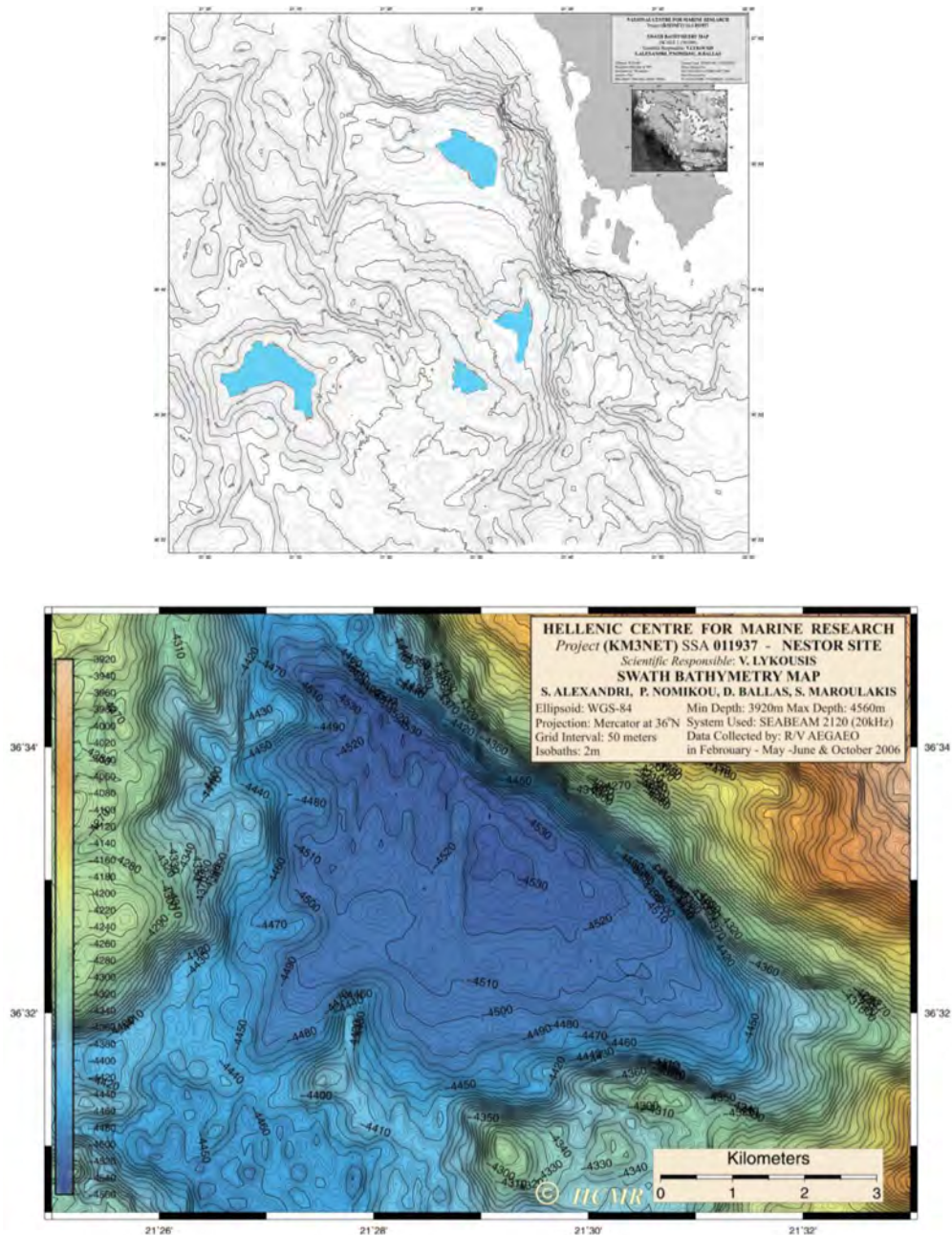

Figure 5-1: Bathymetry maps of the Pylos area. The top panel shows an overview with the 4 possible locations indicated in blue (the northern-most location is 3000 m deep, the others 5200 m, 4500 m and 3750 m (from west to east). Subsequent isobars indicate elevation differences of 50 m. The bottom panel shows a high-resolution map of the 4500 m location; here, subsequent isobars indicate elevation differences of 2 m.
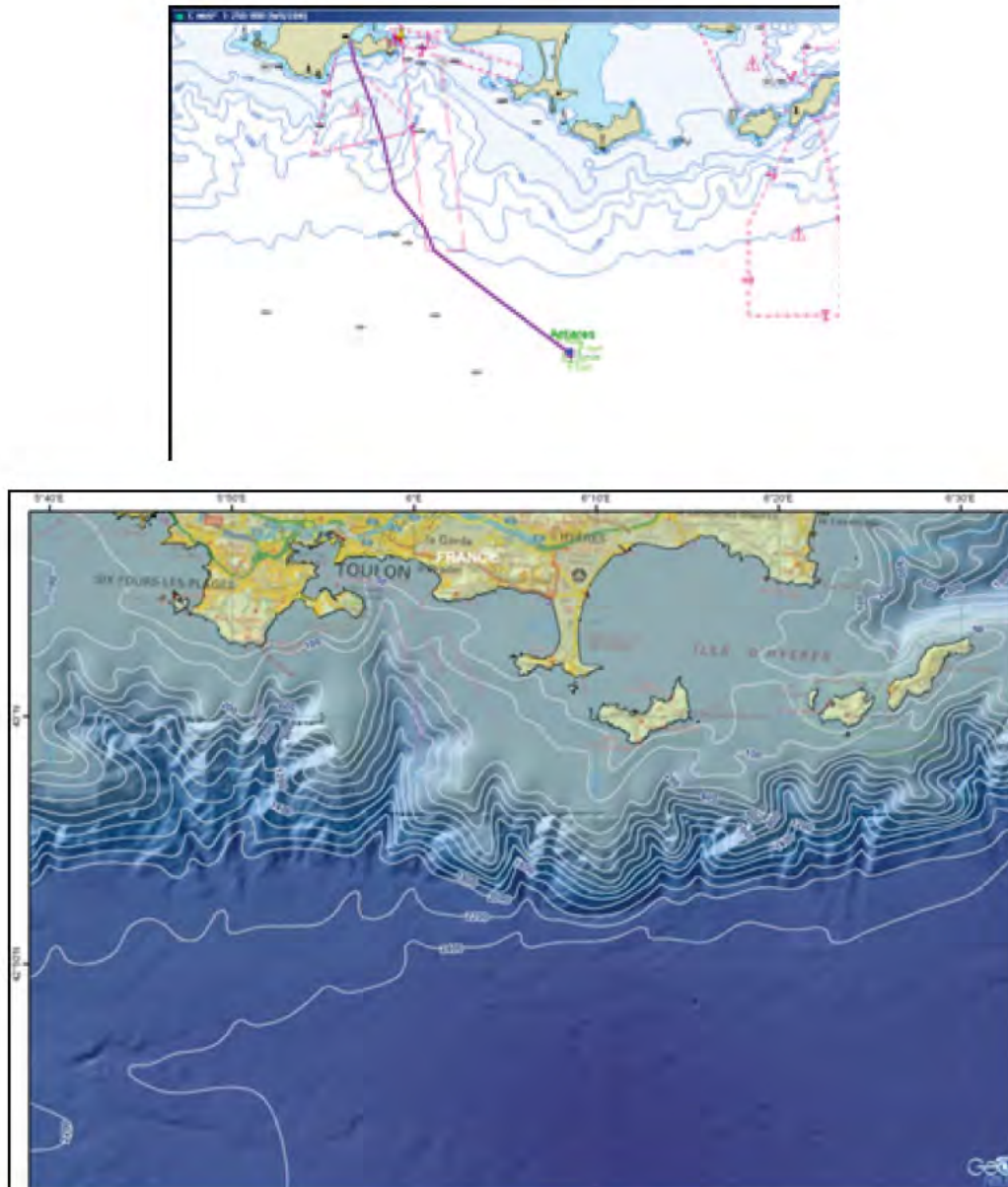
Figure 5-2: Bathymetry map of the Toulon site. The position of the existing ANTARES telescope is indicated on the top map. The lower panel shows a more detailed map of the ANTARES site area.

5.1.2 Weather and Sea Conditions

The weather and in particular the sea state is highly important for deployment operations. Experience of the pilot projects shows that a sea state of 3 at maximum, with wave heights below a metre, is required for safe sea operations. Using modern heave compensation and dynamic positioning technology these requirement could be relaxed to 4 beaufort and 2m waves. The candidate sites provide sufficiently long and frequent periods of calm sea. As examples, Figure 5-3 shows the fraction of time in periods of calm conditions, as a function of the period length, for the Pylos area. Figure 5-4 shows the distribution of wave heights for the Toulon area. It can be concluded that at both sites the sea state is acceptable for deployment operations for more that 50% of the time. The duration of individual deployment operations should be limited to periods of a few days.
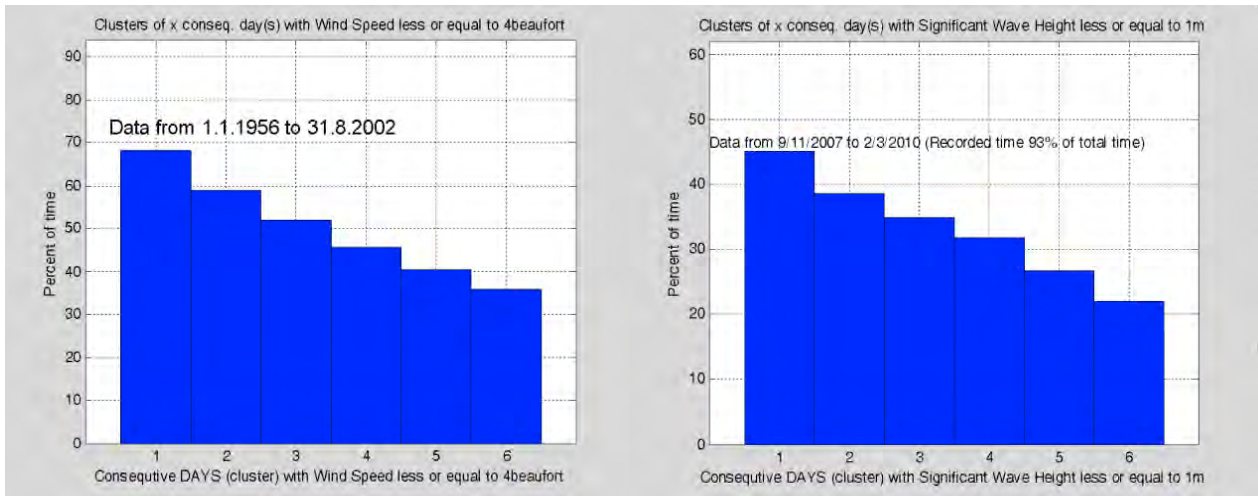
Figure 5-3: Wind speed and sea state conditions at the Pylos site. The left panel shows the fraction of time in periods with wind speed less than or equal to 4 Beaufort (15 knots = 7.9 m/s), as a function of the period length (Source: Greek National Meteorological Service). The corresponding graph for wave heights below 1 m is shown in the right panel. The data are from continuous measurements over 46 years (left) and 29 months (right), respectively. (Source: Hellenic Centre for Marine Research).
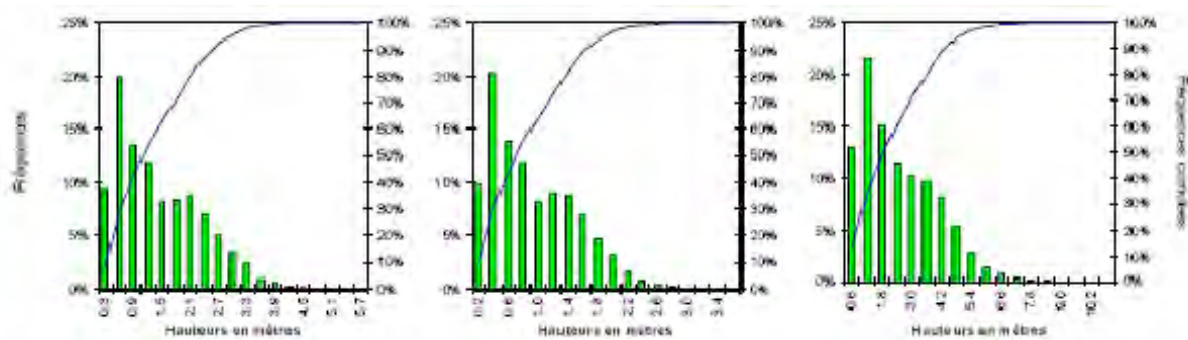

Figure 5-4: Surface wave characteristics at the Toulon site. Shown is the relative abundance of wave heights; the panels from left to right indicate the average height of the 30% largest waves (H1/3); the average wave height; the maximum wave height. The data are from continuous observations over more than 9 years in the period 1992-2001.

5.1.3 Geology

Risks for the operation of the KM3NeT research infrastructure may come from geological processes such as underwater landslides, earthquakes, volcano eruptions or turbidity events. Bore cores of the sediment layer at the sea floor have been taken at all three candidate site areas. Their investigation provided no evidence for major events of these types over the last tens of millennia [26].

5.2 Environmental Site Characteristics

Since the neutrino telescope, as well as the earth and sea science devices, will be operated in the unsheltered natural deep-sea environment, the operation conditions have to be carefully studied to assess their impact on data quality, long-term performance and associated risks.

5.2.1 Temperature

The sea water temperature directly impacts on the temperature at which off-shore components, such as front-end electronics and photomultipliers, are operated. Since their performance typically is temperature-dependent, both local and temporal variations of the water temperature are of concern. Measurements at the different sites have shown that the temperature is stable to within 0.2°C, both as a function of depth (below about 1.5 km) and as a function of time. The average temperature varies from 13.3°C in the Ligurian Sea to 13 5°C in the Ionian Sea.

5.2.2 Salinity

The salt content of the sea water determines its physical and chemical properties, such as conductivity, density and chemical reactivity. These parameters are relevant for KM3NeT as they impact on the design of the telescope. The observed temporal or local salinity variations are small. Measurements show that the salinity in the Mediterranean Sea increases slightly from West to East, from about 38.45 psu[5] at the Toulon site to 38.75 psu at the Pylos site.

Probably the most important aspect of the prevailing salinity value is that it is directly proportional to the potassium (K) content of the sea water, which contributes to the optical background through decays of the natural radioactive isotope 40K. See Sections 6 for more details.

5.2.3 Deep-sea Currents

Since the Detection Units are flexible, the optical modules are displaced from their nominal positions (corresponding to a vertical line shape) due to the drag forces of deep-sea currents. These displacements need to be continuously monitored (see Section 3.5.4), and they have to be limited in magnitude to guarantee the mechanical stability of the detection units (see Section 3.3.5).

Using moorings of current-meters and the ANTARES data, the long-term distribution of current speed and direction has been monitored over several years at all three candidate sites. The results are shown in Figure 5-5 (Toulon), Figure 5-6 (Capo Passero) and Figure 5-7 (Pylos). Whereas for 90% of the time, the current velocity is below 12 (8, 5) cm/s at the Toulon (Capo Passero, Pylos) sites, occurrences of currents with up to about 30 cm/s have been observed at the Toulon site. Any design is therefore required to withstand such currents.

It is known that instabilities of the water column can occur, which are unpredictable in time and location and lead to turbulent downflows of large water masses, causing deep-sea currents of the order 50 cm/s or more. However, no evidence for such events has so far been observed in the candidate site regions over extended measurement periods of up to five years.
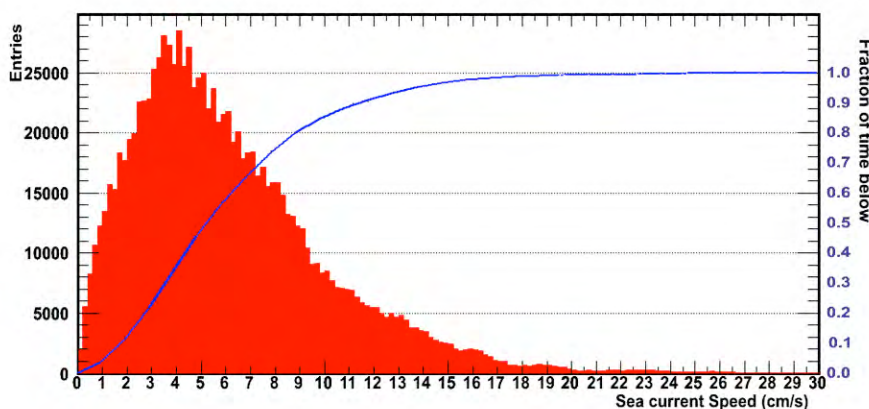

Figure 5-5: Distribution of the deepsea current velocity measured at the Toulon site during the period September 2005 - October 2009 using ANTARES instrumentation. The blue line represents the integrated content of the histogram, normalised to unity.

---

[5] *Practical salinity units, based on conductivity measurements. 1 psu is approximately equal to 1 g of salt per litre of water.*
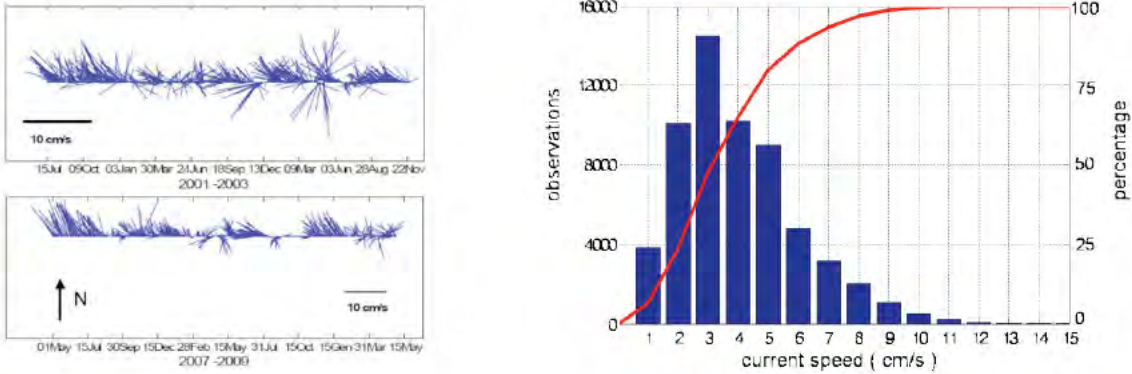
Figure 5-6: Deep-sea current velocities from measurements performed in the periods 2001-2004 and 2007-2009 at the Capo Passero site. The graphs in the left panel indicate the development of direction and speed over time; the plot in the right panel shows the speed distribution (blue histogram) and its integral, normalised to unity (red line). The measurements have been performed at depths up to 500 m above seabed. No significant depth dependence of the currents was observed.
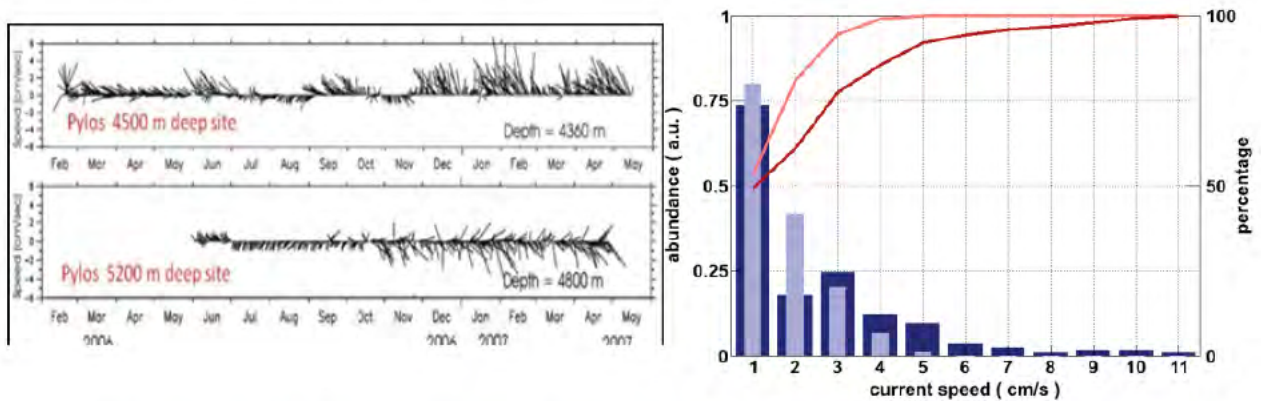

Figure 5-7: Deep-sea current velocities from measurements performed in the period 2006-2007 at the Pylos site. The graphs in the left panel indicate the development of direction and speed over time at the two deepest locations (North is towards the top); the plot in the right panel shows the speed distributions (4500 m: dark blue histogram; 5200 m: light blue) and their integrals, normalised to unity (4500 m: dark red line; 5200 m: light red). Measurements have been made every 8 hours. Velocities measured at intermediate depths between 2000 m and 4000 m show a very similar behaviour.

5.2.4 Sedimentation and Biofouling

The downward flux of sediments can cover the optical modules and reduce the transmittance for Cherenkov light, thus decreasing the neutrino telescope's sensitivity. This effect depends on the angle of view (it is stronger for upward-pointing than for downward-pointing parts of an optical module). It may be supplemented by biofouling, i.e. the growth of a layer of biological organisms (bacteria etc.) on the glass surface, which further reduces the transmittance and in addition provides a "capture ground" for sediments.

The sediment flux has been measured using sediment traps on mooring lines that have been deployed regularly over periods of 1-2 weeks (see e.g. [27,28].) Example results are presented in Figure 5-8. There is a significant seasonal variation in the sediment flux. Even stronger variations are observed from year to year, presumably related to changes of the prevailing weather conditions (in particular wind speed and direction) and to singular occurrences of additional sediment material sources such as ashes from forest fires or sand from the Sahara.
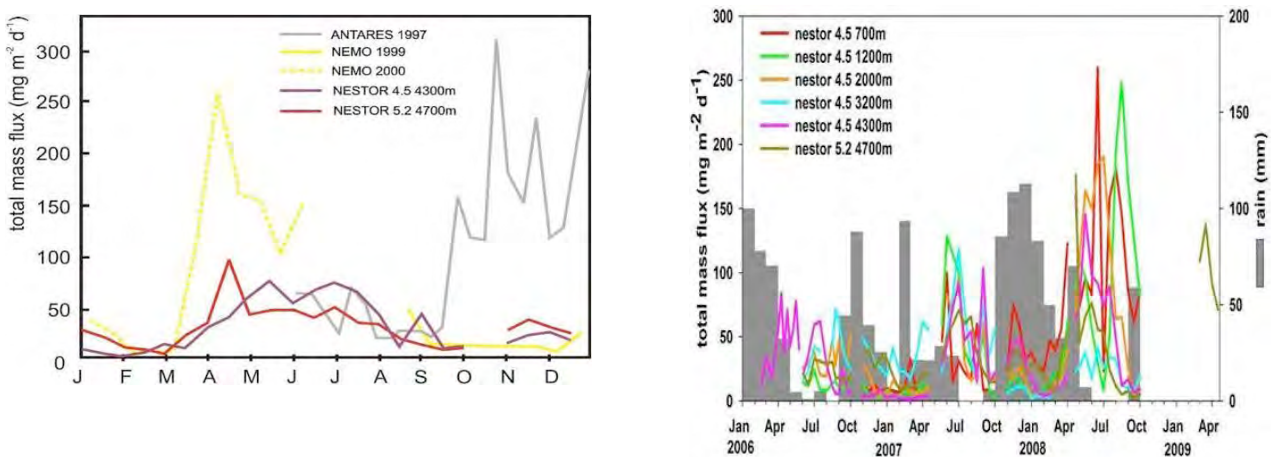

Figure 5-8: Downward total mass fluxes measured at the three candidate sites. The plot in the left panel shows a comparison of the seasonal variation for selected years (averaged over several years for Pylos). In the right panel, the sediment flux as measured at different locations and depths at the Pylos site during the period 2006-2009 is shown. Times and intensity of precipitation are also indicated.

Longer-term average rates of sedimentation can be inferred from the bore cores. The results are 0 2-0 5 mm/year for the Toulon site, about 0.04 mm/year for Capo Passero and 0.02 mm/year for Pylos [26,29].

The combined effect of sedimentation and biofouling on the transmittance of optical modules has been investigated in long-term measurements with dedicated instruments. In Figure 5-9, the LIMS[6] device [30] is presented as an example; 20 LIMS instruments have been produced and operated from May 2007 to October 2009 (260 LIMS-months). The measurement principle is to instrument the inner surface of an optical module with light sensors at positions corresponding to different polar angles and monitoring their response to external light sources at fixed positions and with constant intensity.

Typical data retrieved from these measurements are shown in Figure 5-10 for the Pylos site and in Figure 5-11 for the Toulon site (from a similar device deployed earlier by the ANTARES collaboration [27]). The measured reduction rates of transmittance are shown in Figure 5-12 as functions of the polar angle. In all sites, these rates roughly coincide for downward directions between nadir and horizontal (a few percent reduction per year), but they somewhat differ for upward directions of view, as to be expected from the different sedimentation rates.

It is to be noted that during and after periods of stronger currents an increase of the transmittance was observed (see Figure 5-11), indicating that the biofouling and sedimentation layer is washed off to some extent.

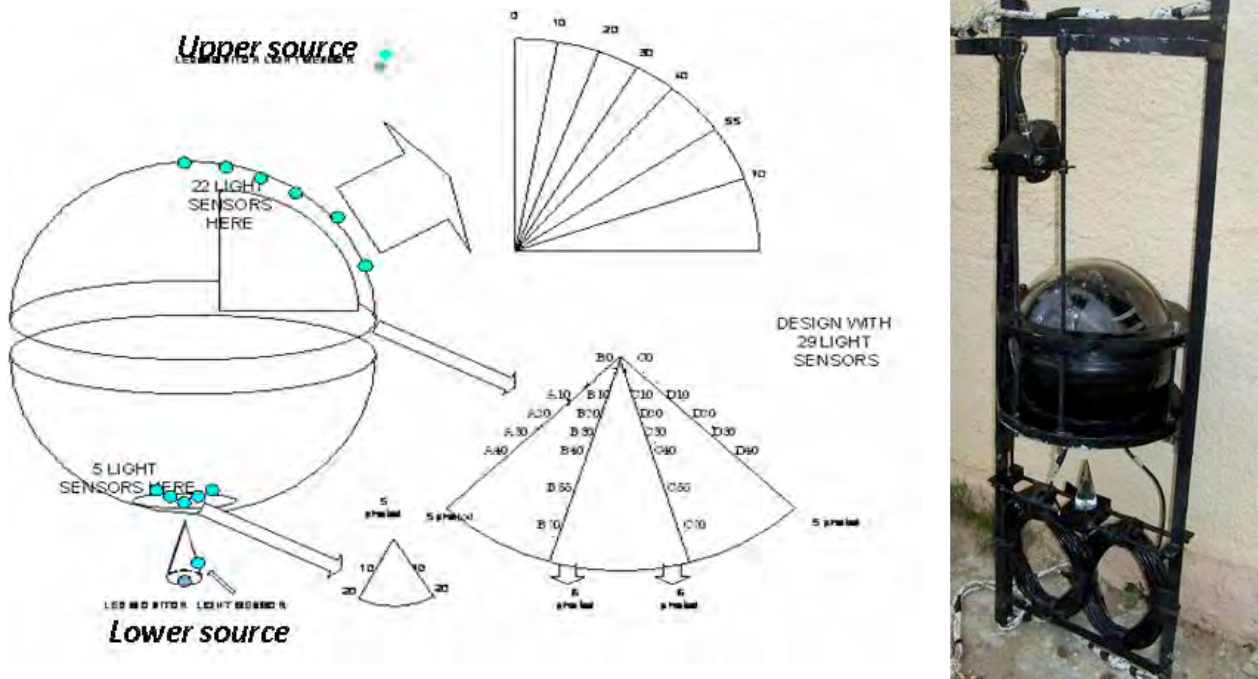
[6] *Light Intensity Measuring Device.*

Figure 5-9: The LIMS instrument for long-term transmittance measurements. The left panel shows the geometry of light sources and sensors placed inside a glass sphere as used for optical modules. 22 sensors are upwards-pointing at zenith angles between 0° and 70°, 5 sensors are installed close to the nadir (180°). Two light sources are operated alternating to illuminate the upper and the lower part of the sphere. The right panel shows a LIMS instrument ready for deployment.
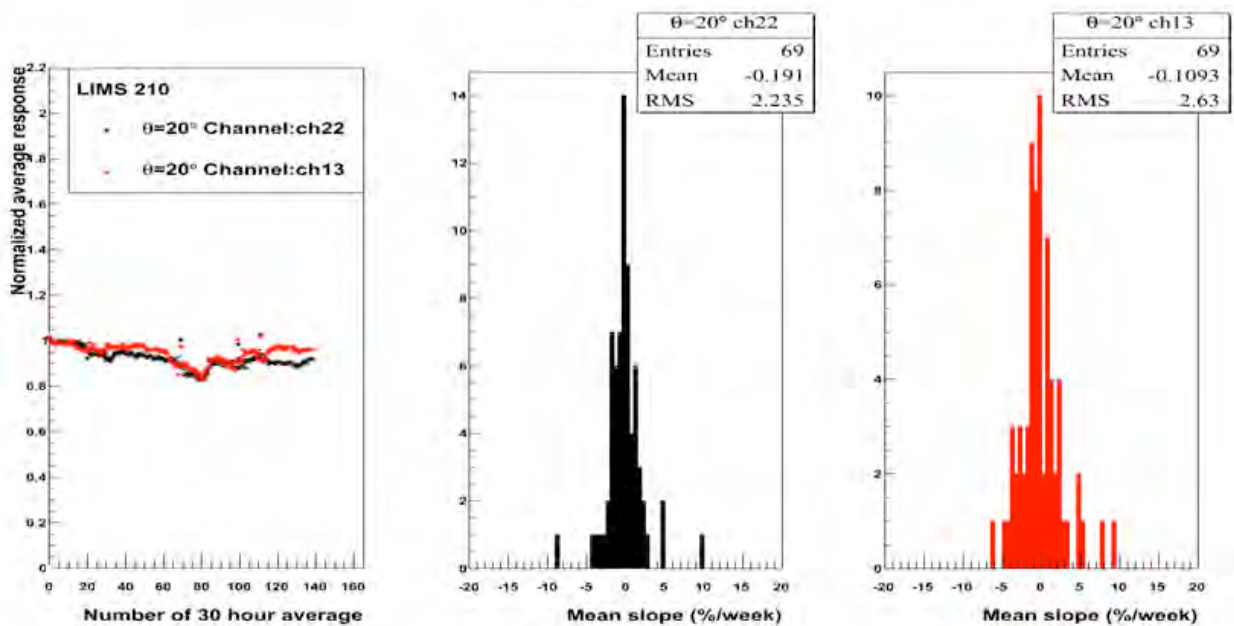

Figure 5-10: Typical example data taken with a LIMS device over a 6-month period at the Pylos site, at a depth of 3240 m. The data of two sensors, averaged over 30-hour periods and normalised to unity at the start of the measurement, are shown in the left panel. The middle and right panels show the distribution of weekly variations in percent of the corresponding transmittances.
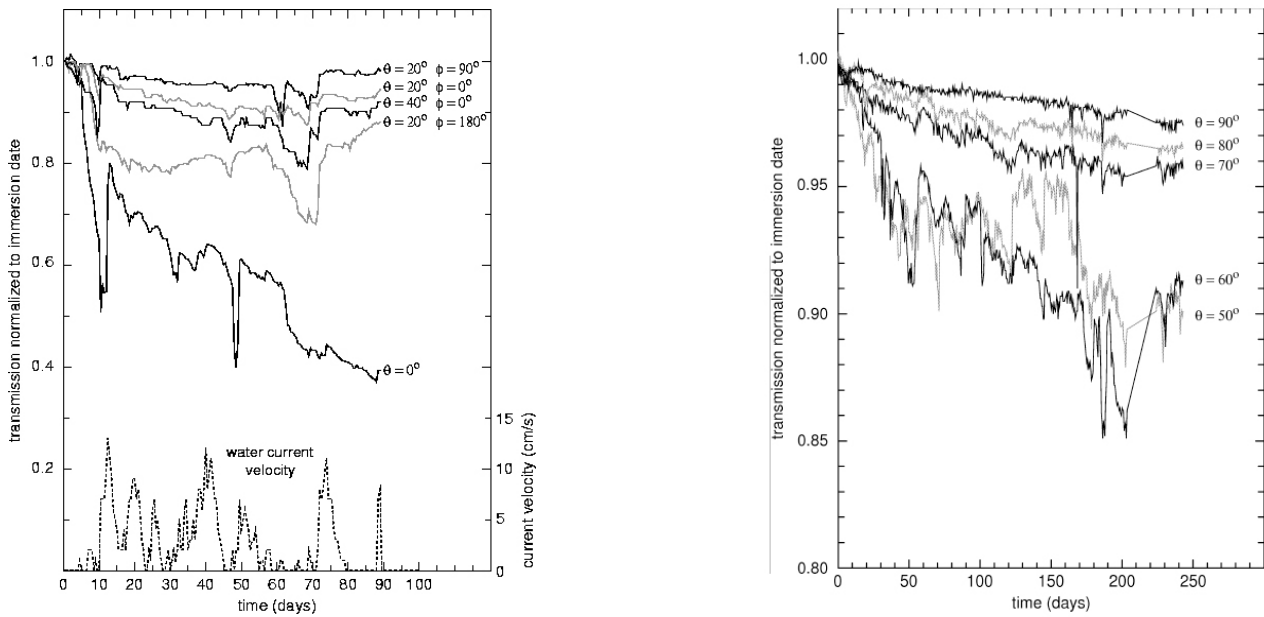
Figure 5-11: Time dependence of transmittance measured at the Toulon site in two campaigns in 1997-1998. The left panel shows the results of a 3-month measurement with the sphere illuminated from above; the right panel is from a 8-month period, where the illumination was horizontal. The θ values indicate the zenith angles of the photo-sensors inside the sphere. The water current speed is indicated for the first measurement.
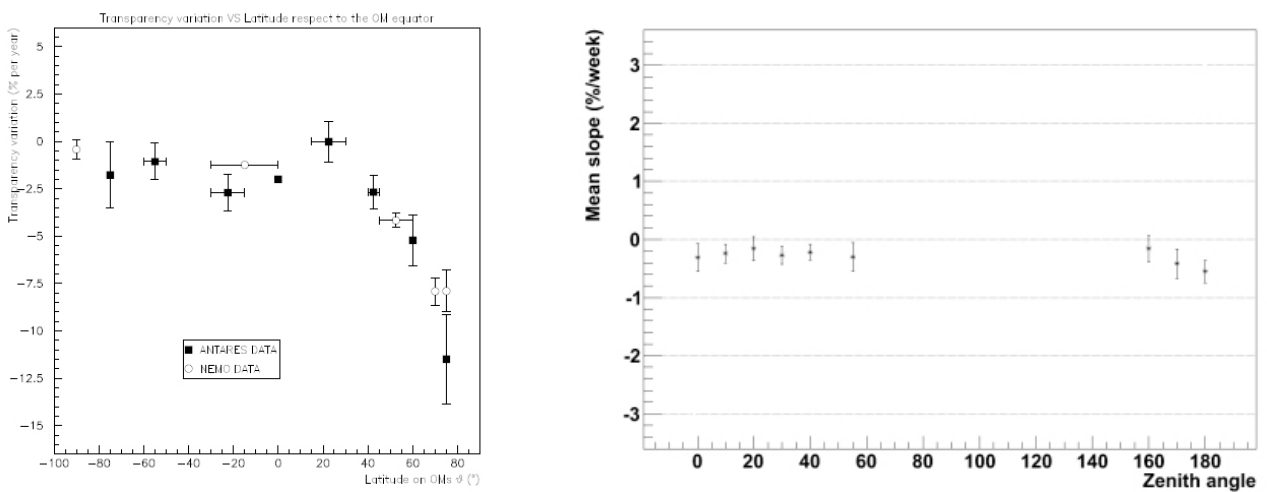

Figure 5-12: Decrease of transmittance with time. The left panel shows a comparison of measurements at the Toulon (black squares) and the Capo Passero (open circles) sites. The polar angle is given as latitude (-90° is downwards-looking, 90° is upwards-looking). The right panel shows results obtained with LIMS at the Pylos site in 3240 m depth.

A growth of peculiar organisms was observed when recovering an ANTARES detection unit after 2.5 years in the deep sea. The exact classification and properties of these organisms, the conditions for their growth, their abundance throughout the Mediterranean, as well as longer-term investigations of their impact on the neutrino telescope performance need to be further investigated. The transmittance reduction after the 2.5 years due to this growth is of the order of 1% and thus has no significant adverse effect on the sensitivity of the neutrino telescope. Other spheres have been recovered at this and the other sites after similar time in the deep sea and have shown no growth.

5.2.5 Radioactivity

Radioactive β and γ decays in the sea water cause continuous, homogeneous and isotropic emission of Cherenkov light. The dominant contribution to this background light is from ^{40}K decays. The K concentration in sea water is 0.010 mol/litre; the relative abundance of ^{40}K is 0.012% and its half-life 1.25×10^9 years. The resulting activity is about 13 Bq/litre, causing a typical count rate of 40 kHz on an 8-inch photomultiplier (threshold at 0.3 photo-electrons). In order to investigate possible additional contributions or temporal variations of this rate due to other radio-nuclides, in particular from anthropogenic sources, a radioactivity probe (see Figure 5-13) was constructed and deployed at the Capo Passero site for 6 months. The probe uses a NaI(Tl) crystal to measure the γ spectrum of radioactive decays in sea water. The expected activity level from ^{40}K decays was confirmed (see Figure 5-14) and no significant additional activity rates were observed. Water samples from the Pylos site have been collected and analysed in the laboratory. Also here, the ^{40}K activity was confirmed (14 ± 1 Bq/litre) and the overall activity from anthropogenic isotopes (^{137}Cs, ^{243}U, ^{238}U) found to be of the order of 0.05 Bq/litre.

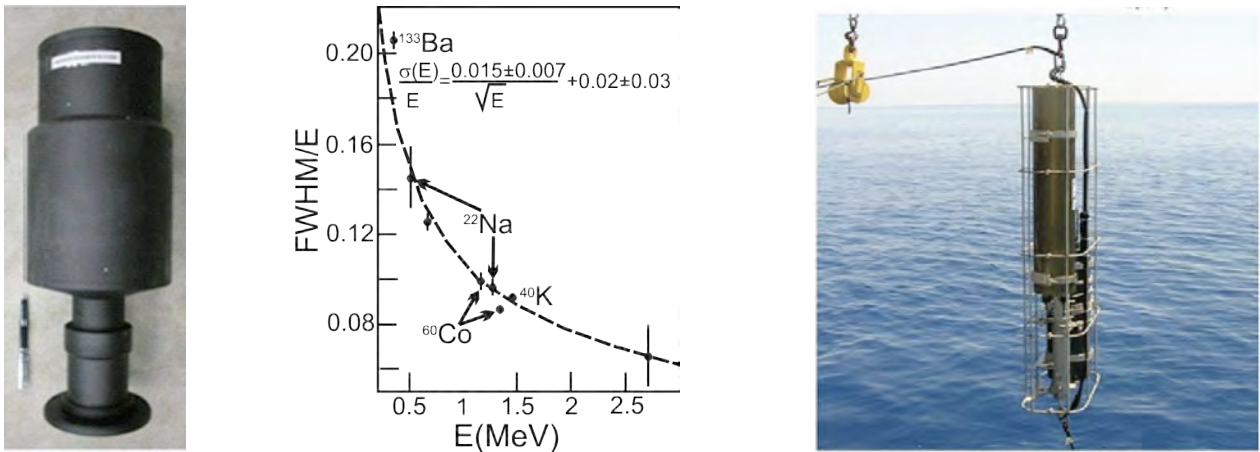$$\frac{\sigma(E)}{E} = \frac{0.015 \pm 0.007}{\sqrt{E}} + 0.02 \pm 0.03$$

Figure 5-13: The gamma spectrometer developed for gamma activity measurements in the deep sea. The left panel shows a photograph of the instrument, the middle panel the result of calibration obtained with radioactive sources and the right panel the instrument during deployment as part of a mooring operated for six months at the Capo Passero site.
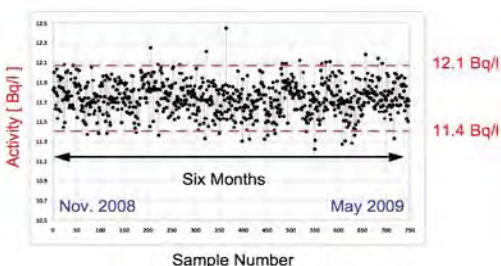

Figure 5-14: ^{40}K activity at the Capo Passero site, measured over 6 months using the radioactivity probe shown in Figure 5-13. The measurement is based on the γ decay mode of ^{40}K.

126

5.2.6 Bioluminescent Organisms

Further sources of background light are bioluminescent organisms, which typically emit light in the blue wavelength regime, where water has maximal transparency [31,32]. There are two contributions to bioluminescent light, one varying on time scales of hours to days (presumably from bacteria) and one coming in "bursts" with durations of a few tenths to a few tens of seconds (assigned to larger organisms). The photomultiplier count rate from the steady component can be of similar size as that from ^{40}K and is typically homogeneous over the full detector; a burst can cause rates that are larger by orders of magnitude, but affect only a local group of optical modules. Both components thus differ significantly in their impact on data taking, filtering and analysis (see Section 6.1).

The most direct assessment of bioluminescence and its impact on the neutrino telescope is by measuring the intensities of deep-sea background light over long-term periods. The corresponding results are presented in Section 5.3.3.

To investigate the occurrence of bioluminescent organisms, water samples have been retrieved from different depths at a location near the Capo Passero site. Subsequently, the density of luminescent bacteria cultivatable at atmospheric pressure has been determined. The results (see Figure 5-15) indicate that such bacteria are essentially absent at depths beyond 2500 m [28].

To compare the abundance of bioluminescent animals at the Capo Passero and Pylos sites measurements were made with the ICDeep camera (I²CCD (Image Intensified Charge Coupled Device) for Deep-sea research). Measurements were made in autumn 2008 and spring 2009 to investigate seasonal changes at each site. The ICDeep camera is more sensitive than the ISIT camera, which was used for previous measurements at the Pylos and Ligurian sea sites[33,34] resulting in higher abundance values.

A seasonal effect was found at the Capo Passero site where abundance values were higher in the autumn than in spring between 500-2400 m depth. No seasonal effect in the abundance of bioluminescent animals was found at the Pylos site. Comparing the two sites higher abundance values are found at the Capo Passero site in spring and autumn than at the Pylos site (Fig XX). In water 2500-3500 m densities of bioluminescent animals were 2-3 times higher at the Capo Passero site (0.4-0.6 m^{-3} in autumn and spring, respectively) than the Pylos site (0.24 – 0.17 m^{-3})
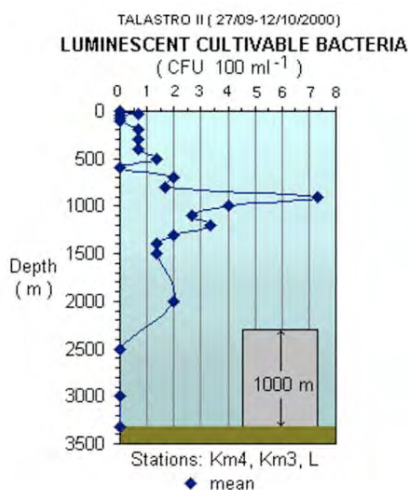
Figure 5-15: Concentration of luminescent bacteria cultivatable at atmospheric pressure, as a function of depth. The data have been obtained from water samples taken at the Capo Passero site.
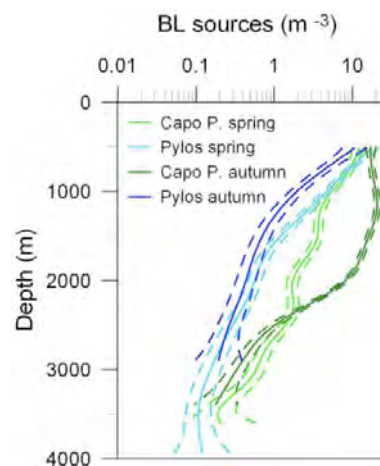
Figure 5-16: Density of bioluminescent animals at the Capo Passero and Pylos sites, in autumn 2008 and spring 2009. (Dashed lines show 95% c.l.)

127

5.3 Optical Properties of the Deep-Sea Environment

The study of the deep-sea water optical properties has been performed through a long-term programme carried out spanning all seasons. Sea water absorbs and scatters light depending on the water temperature, salinity, as well as the characteristics and concentration of the suspended particulate. These parameters are different at different marine sites and may vary as a function of time. Furthermore, the intensity and time dependence of background light from radioactivity and bioluminescence (Section 5.3.3) has been measured in long-term exploratory campaigns and by the ANTARES experiment and is reported in the following.

5.3.1 Light Transmission Parameters

Light transmission through media is affected by absorption and scattering. Scattering processes in which only the direction of the light is changed are dominant, whereas scattering phenomena in which also the photon wavelength changes (e.g. the Raman effect) happen less frequently. Scattering can take place either on molecules (Rayleigh scattering) or on particulate matter (Mie scattering). In order to properly describe the transparency of sea water as a function of wavelength, it is necessary to measure the parameters describing absorption and scattering, such as the absorption length $L_a(\lambda)$ scattering length $L_b(\lambda)$ and attenuation length $1/L_c(\lambda) = 1/L_a(\lambda) + 1/L_b(\lambda)$. Each of these lengths represents the path after which a beam of initial intensity I_0 and wavelength λ is reduced in intensity by a factor of 1/e through absorption, scattering or both according to

$$I_{a,b,c}(x) = I_0 e^{\left(-\frac{x}{L_{a,b,c}}\right)}$$

where x is the optical path traversed by the beam. In the literature, also the coefficients of absorption, $a = 1/L_a(\lambda)$, and scattering, $b = 1/L_b(\lambda)$, are used to characterise the light transmission through matter. The sum of scattering and absorption coefficients is called attenuation coefficient c. Other parameters commonly used in the literature are the effective scattering length

$$L_b^{eff} = \frac{L_b(\lambda)}{1 - \langle \cos\vartheta \rangle} = \frac{1}{b_{eff}}$$

and the effective attenuation length

$$L_c^{eff} = \frac{1}{c^{eff}} = \frac{1}{a + b^{eff}},$$

where $\langle \cos\vartheta \rangle$ is the average cosine of the scattering angle. The estimation of the latter parameter is difficult since it needs the knowledge of another inherent optical property, the volume scattering function $b(\vartheta)$, which must be measured with appropriate devices. Using an isotropic light source, it is also possible to measure the so-called transmission length, $L_\beta(\lambda)$ characterising the variation of light intensity as a function of the distance, R, between the source and the detector:

$$I(\lambda, R) = \frac{I_0(\lambda)}{4\pi R^2} e^{-\frac{R}{L_\beta(\lambda)}}$$

The transmission length can be determined, for specific values of λ, by fitting $I(\lambda,R)$ to data taken with fixed $I_0(\lambda)$ and several values of R.

A direct comparison between measured values of $L_\beta(\lambda)$ and L_c^{eff} requires the knowledge of the volume scattering function as a function of λ, or of the value of $\langle \cos\vartheta \rangle$. This knowledge is still lacking for the Mediterranean Sea.

5.3.2 Light Transmission Measurements

The Toulon site has been studied for many years with dedicated setups designed to characterise water optical properties. Early measurements [35] taken between 1997 and 2000 were made for blue (473 nm, with 10 nm of FWHM) and UV (375 nm, with 10 nm of FWHM) light. The resulting absorption, scattering, and effective attenuation lengths are summarised in Table 5.1 and Table 5.2 .

Using data from the ANTARES instrumentation, the transmission length is being monitored continuously since 2008. Light signals from optical beacons (wavelengths 400 and 470 nm, operated periodically for calibration purposes) registered by optical modules placed at various distances allow for measuring in situ the light transmission as a function of distance. Figure 5-17 shows the results of these measurements. Monte Carlo simulations indicate that, for reasonable scattering models, the absorption length at 470 nm is typically 5 m larger than the transmission length.

Date	Effective attenuation length (m)	Absorption length (m)	Effective scattering length (m)
July 1998	60.6 ± 0.4 ± 5	68.6 ± 1 3 ± 5	265 ± 4 ± 28
Mar. 1999	51.9 ± 0.7 ± 1	61.2 ± 0.7 ± 1	228 ± 11 ± 24
June 2000	46.4 ± 1.9 ± 2	49.3 ± 0 3 ± 2	301 ± 3 ± 27

Table 5.1: Water optical properties measured at the Toulon site using blue light (λ =470nm). The first error is statistical and the second one is systematic.

Date	Effective attenuation length (m)	Absorption length (m)	Effective scattering length (m)
July 1999	21.9 ± 0.8 ± 2	23.5 ± 0.1 ± 2	119 ± 2 ± 10
Sept.1999	22.8 ± 0.3 ± 2	25.6 ± 0 2 ± 2	113 ± 3 ± 10
June 2000	26.0 ± 0.5 ± 1	28.9 ± 0.1 ± 1	133 ± 3 ± 12

Table 5.2: Water optical properties measured at the Toulon site using UV light (λ =375 nm). The first error is statistical and the second one is systematic.
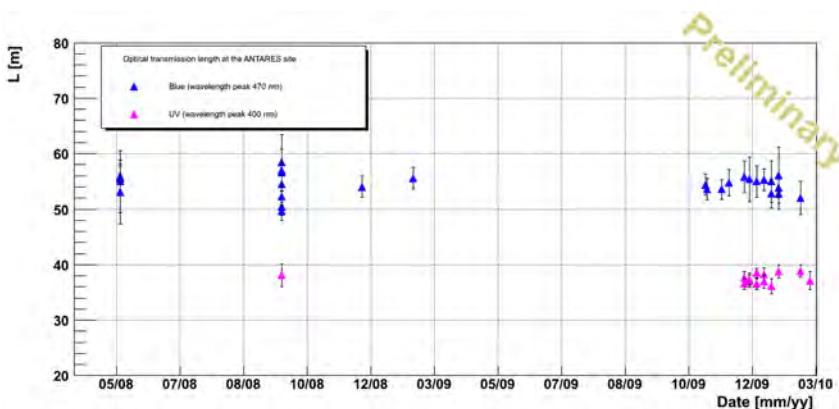

Figure 5-17: Results of in situ measurements of the transmission length at the Toulon site. The Measurements were performed using ANTARES instrumentation. The blue symbols are for a wavelength of 470 nm, the magenta ones for 400 nm.

The light transmission at the Capo Passero site has been investigated [36] using a setup including a commercial instrument (the AC9 by WETLABS) capable of measuring, in a collimated geometry, the absorption and the attenuation coefficients for nine wavelengths ranging from 410 nm to 715 nm. The values of the absorption and attenuation lengths have been determined for each measurement by averaging the data for depths greater than 2850 m [37]. The results of four sets of measurements taken in different seasons are shown in Figure 5-18. For comparison, light absorption and attenuation data for optically pure sea water [38] are also shown. At all wavelengths, deep waters at that location have an absorption length compatible with that of pure sea water. There is no evidence of a seasonal dependence of the optical parameters.

The NESTOR group has developed and operated a device (Long-Arm Marine Spectrophotometer, LAMS) to determine the transmission length by means of a rigid structure that allows for measuring the intensity of light from an isotropic, constant source at distances of R=10, 15, 17, 22 m (see Figure 5-19). Measurements have been performed at 8 wavelengths ranging from 376 nm to 520 nm and at different depths, at the Pylos and Capo Passero sites.

Table 5 3 shows a comparison of the corresponding results, for similar depths and at about 200 m above seabed at both sites. More details can be found in [39]. The transmission length measured by LAMS cannot easily be related to absorption or attenuation length (see Section 5.3.1). The transmission length was previously measured at different locations in the Pylos area using a non-collimated light source at a wavelength of 460 nm; a result of 55 ± 10 m was found[40].

The results in Table 5.3 indicate a transmission length that is roughly 10% larger at the Pylos than at the Capo Passero site; however, it must be noted that these measurements represent a snapshot at a given time (the campaign at both sites was performed within a few days) and the systematic uncertainties quoted do not account for longer-term variations of the respective optical properties.
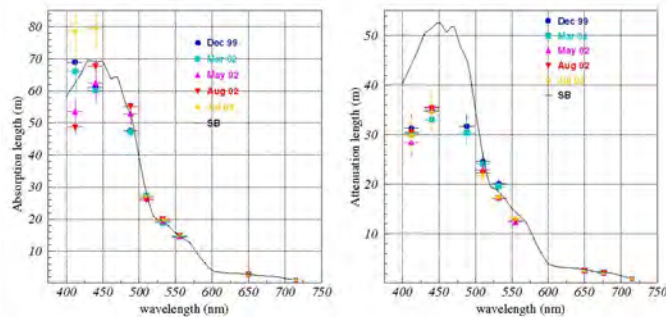

Figure 5-18: Absorption length (left panel) and attenuation length (right panel) measured at the Capo Passero site at four seasons. Also indicated are the the values for optically clean salt water (black lines). Figure taken from [36].
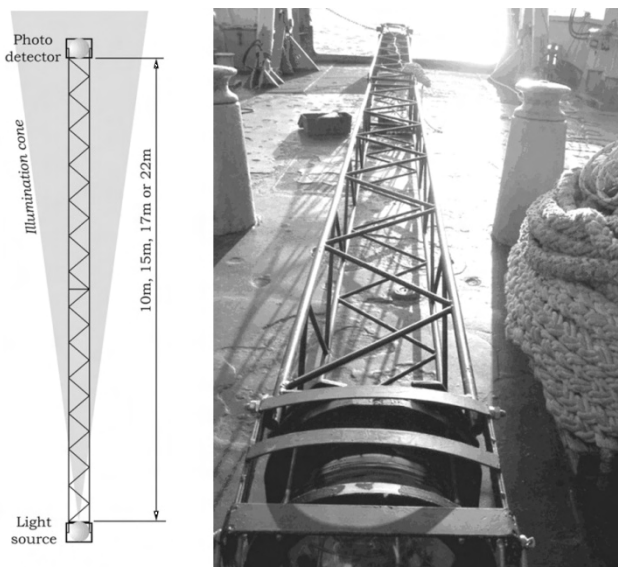

Figure 5-19: Schematic of the LAMS instrument (left), and photographs of it shortly before deployment (upper right) and during deployment (test operation with green light, lower right).

Site	Depth m	376 nm	386 nm	400 nm	425 nm	445 nm	463 nm	502 nm	520 nm
N4.5	4100	21.0±0.5	24.8±0.7	29.2±0.9	36.0±1 3	42.3±1.8	46.1±2.0	28.7±0.8	21.3±0.5
CP2	3400	18.6±0.4	21.8±0.5	25.6±0.7	32.4±1.1	38.5±1.5	42.0±1.7	27.1±0.8	20.9±0.5
N4.5	3000	21.9±0.5	25.7±0.7	30.5±1.0	37.8±1 5	43.8±1.9	47.2±2.2	29.3±0.9	21.5±0.6
CP1	3100	19.9±0.4	23.2±0.6	27.8±0.8	34.6±1 2	41.5±1.7	44.1±1.9	28.5±0.8	21.8±0.5
CP2	3000	19.5±0.4	23.0±0.5	27.3±0.8	34.1±1 2	39.6±1.6	43.7±1.8	27.6±0.8	21.1±0.5

Table 5.3: Transmission lengths (in metres) for light of different wavelengths at Pylos (N4.5), and Capo Passero (CP1 and CP2) sites for the largest and similar depths.

5.3.3 Background Light Measurements

Before detector construction, the ANTARES Collaboration performed a series of in situ measurements of the background light in the Toulon site using 8-inch photomultiplier tubes on autonomous device systems[41]. These measurements revealed the two contributions to the optical background described above: a continuous base rate ("baseline") of a few tens of kHz, varying slowly on time scales of a few hours, and sharp peaks lasting a few seconds and rising to tens of MHz ("bursts"). A typical time stream of data, acquired in April 2005 [42]., and the median counting rate of single optical modules during almost 5 year are shown in Figure 5-20. Counting rates were acquired with a threshold of 0 3 photoelectrons. The two components of optical background described above are clearly visible.
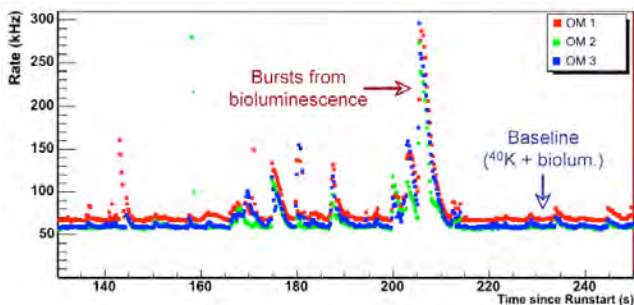

Figure 5-20: Upper panel: Counting rates in three optical modules of an ANTARES storey over a period of 4 minutes. The small differences in the baseline are due to slightly different sensitivities of the photomultipliers. Lower panel: Median counting rates in different ANTARES optical modules over a period of almost 5 years. The colours indicate different optical modules.
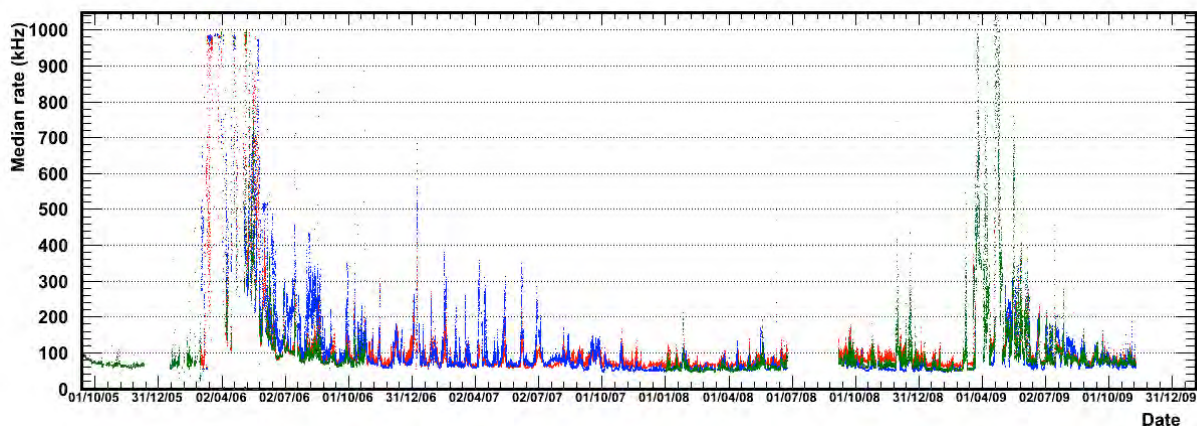
The baseline component is neither correlated with the sea current, nor with the burst frequency; however, long-term variations of the baseline rate were observed in the ANTARES detector. Periods of high burst activity are uncorrelated with variations of the baseline component, suggesting that each of the two contributions is caused by a different population. Moreover, a strong correlation is observed between burst activity and the current velocity, as shown in Figure 5-21 [43].

Optical background data in Capo Passero were collected by means of two different setups. One, built by the NEMO Collaboration, consisted of two 8-inch photomultipliers and the associated electronics, the second, built by the ANTARES Collaboration, used an optical module containing a 10-inch photomultiplier. The two devices have been used to collect data separately, but also together in order to assess systematic uncertainties. Figure 5-22 shows the photomultiplier count rate as a function of time, as obtained with the NEMO setup [28] using a threshold equivalent to 0.33 photo-electrons. After subtracting the dark count rate of 7 kHz an average counting rate of $28.4 \pm 2 5$ kHz is obtained. This background is rather constant and shows only rare bioluminescence bursts. From this rate, taking into account the properties of the optical module and the photomultiplier, an isotropic photon flux of 360 ± 40 cm^{-2}s^{-1} in the wavelength range of sensitivity of a bi-alkali photocathode is derived. This flux is consistent with the expectation from just the ^{40}K decays.
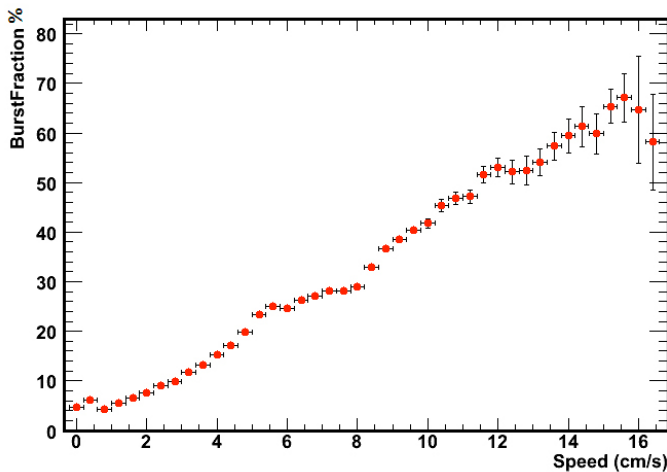

Figure 5-21: Correlation of burst fraction (the fraction of time with count rates exceeding 120% of the baseline rate) and deep-sea current speed. The data have been collected with the ANTARES detector from summer 2005 to summer 2006 at the Toulon site.
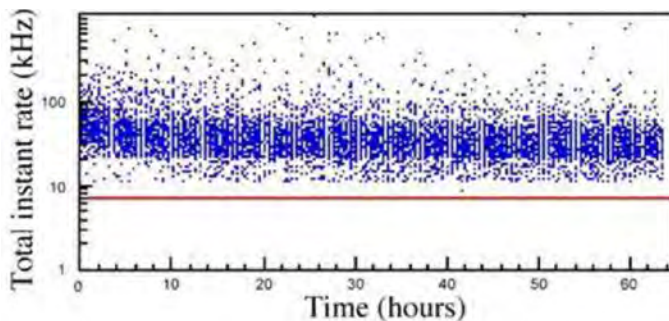

Figure 5-22: Count rate of a single 8-inch photomultiplier at the Capo Passero site, for a measurement period of approximately 3 days. The threshold was set to 0.33 photoelectrons. The red line indicates the dark current count rate.

Also in the Pylos area the optical noise has been measured on several occasions and with different devices. A number of free-drop experiments have been performed since 1996, at a depth of 4000 m, with an apparatus composed of two optical modules. The NESTOR floor deployed and operated in 2003 was also used to study the optical background [44]. A data sample of 100 s duration is shown in Figure 5-23 [45]. From the analysis of the full data sample it is concluded that bioluminescence occurs during 1.1% ± 0.1% of the time, consistent with earlier measurements using autonomous optical modules.
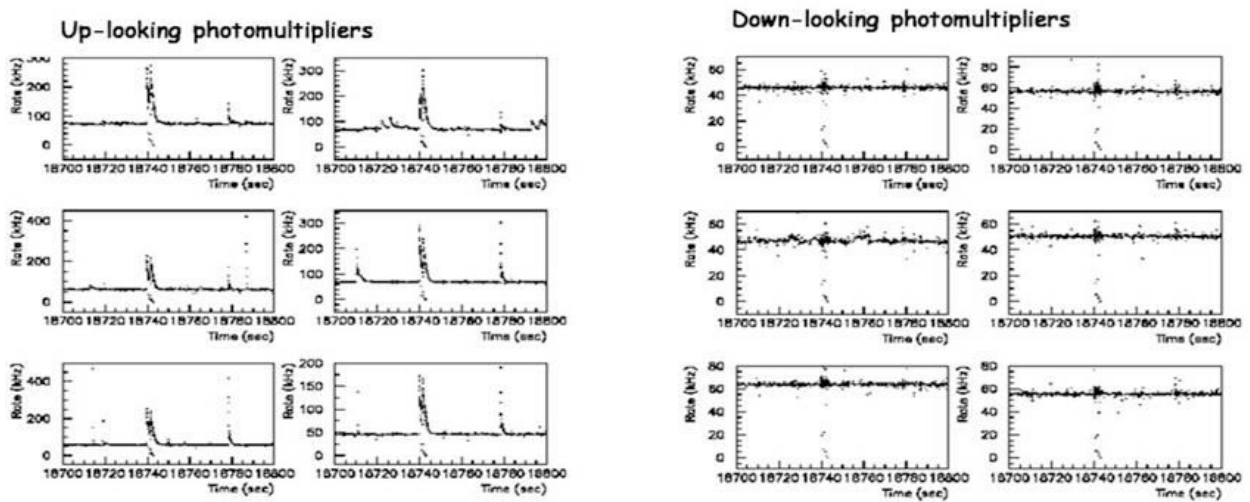

Figure 5-23: Count rates measured with the 12 optical modules of the NESTOR floor operated in 2003. A period of 100 s is covered.